Development of a Combined Cohesive and Virtual Crack-Closure Technique Approach to Represent R-Curves

Daniel A. Drake[1], Carlos G. Dávila[1], and Cheryl A. Rose[1]

[1] NASA Langley Research Center, Hampton, VA 23681, U.S.A.

Abstract. Resistance curve (R-curve) effects due to fiber bridging, crack migration, and other blunting mechanisms are common in composite laminates. These mechanisms can dramatically increase the resistance to crack propagation but can be challenging to simulate. Delamination with R-curves can be analyzed using cohesive zone modeling (CZM) or the virtual crack closure technique (VCCT). Large fracture process zones can be simulated with CZM, but they require highly refined meshes. Coarser meshes can be used with VCCT, but this method is only applicable to small fracture process zones with R-curves defined as functions of position. Therefore, a technique with the computational efficiency of VCCT and the natural ability of cohesive elements to represent large fracture process zones is desirable. An approach is proposed that starts as a CZM in which the cohesive traction separation law (TSL) is separated into high-strength (HS) and low-strength (LS) components. The HS part, which is responsible for the mesh requirements of the CZM analysis, is replaced by VCCT. The combined method is evaluated by analyzing the response of double cantilevered beam specimens. Two specimen layup configurations, $[0/90/90/0]_{3s}$ and $[0/90/90/0]_{9s}$, are evaluated. The R-curve response from each configuration is determined and applied to the constitutive properties of models built with CZM and with VCCT. The results and computational efficiency of the CZM, VCCT, and combined approaches are compared. The results are indicative that a combined cohesive/VCCT approach can enable progressive failure analyses to retain the computational efficiency of VCCT with the ability of the cohesive elements to capture R-curve effects.

Keywords: Virtual Crack-Closure Technique, Cohesive Zone Modeling, Delamination.

1 Introduction

Of all the failure mechanisms that can occur in polymer composite laminates, interlaminar fracture, or delamination between the plies, has received the most attention because it can occur at relatively low out-of-plane loads as compared to loads resulting in other failure mechanisms (i.e., intralaminar or translaminar fracture). Initiation and propagation of delamination are highly influenced by resin ductility, crack migration events, and blunting mechanisms due to fiber bridging from weak fiber/matrix interfaces and through-the-thickness reinforcements [1]. Such phenomena can significantly increase the resistance to delamination propagation and result in increases in the strain energy

release rate (SERR), or R-curve effects, with respect to delamination growth. These R-curve effects are indicative of finite fracture process zones that are not accounted for using linear-elastic theory, which assumes an infinitesimally small fracture process zone.

Considerable progress has been made in developing finite element methodologies to simulate delamination within composites, such as cohesive zone modeling (CZM) [2] and the virtual crack-closure technique (VCCT) [3]. Using a CZM approach, small cohesive element sizes (< 0.1 mm) are often necessary to estimate the fracture process zones during delamination because of the low matrix ductility and high strength typically observed in aerospace-grade composites. As a result, the computational time to complete a simulation is high because a large number of elements and degrees of freedom (DOF) are needed. In contrast, the VCCT is a computationally efficient approach that can use notably greater element sizes (> 10 mm) than those needed for CZMs [3, 4].

The VCCT is a linear elastic fracture mechanics (LEFM) approach that is used to estimate the SERR of a cracked body based on nodal forces and opening displacements that are located near the crack tip [3]. To model the delamination growth, the nodal pairs are gradually or instantaneously released along the crack path after the SERR reaches a critical value (fracture toughness). Infinitesimally small fracture process zones are assumed using the VCCT approach during the initiation and propagation of delamination. It is possible to simulate R-curve effects by specifying increasing values of the critical SERR along the path of propagation. Since R-curves depend on the structural configuration, representing them as a function of position implies several limitations. It would therefore be desirable to represent these R-curve effects as material properties of the physical bridging that occurs between the laminates.

The objective of the effort presented herein is to evaluate a procedure that combines the advantages of VCCT and CZM. In this study, double cantilevered beam (DCB) tests with carbon/epoxy composite specimens of different thicknesses are experimentally evaluated to determine their R-curve response. Three different finite element models (a VCCT model, a CZM model, and a VCCT/CZM model) are developed and the analysis results are compared to corresponding experimental data. In the next section of this paper, the use of superposition of bilinear cohesive elements to reproduce R-curve responses is described, which is followed by the description of using the VCCT approach and combined VCCT/CZM approach. These sections are followed by a description of the material system, experimental procedure, and computational approach. Lastly, a discussion of the results is presented.

2 Representing an R-curve response with CZM

The CZM approach utilizes traction-separation laws (TSLs) to represent the initiation and propagation of delamination growth. The shape of the TSL describes the elastic and softening responses of an interface as a function of the opening displacement at the crack front. The area under the TSL is equal to the critical SERR (G_c) and the peak value is the strength of the interface (σ_{c0}). The process zone in a cohesive analysis is

the region of partially damaged elements that span from the leading crack tip (damage variable, $d \approx 0$) to the lagging crack tip ($d \approx 1$). In problems where the length of the process zone (l_{pz}) is small compared to the critical structural dimensions, LEFM is applicable and crack propagation is dominated by G_c. When l_{pz} is large, the leading crack tip leaves in its wake a process zone that bridges the crack faces and thus contributes to the resistance to further propagation. Under these conditions, the shape of the TSL is important: a concave TSL with a larger critical opening displacements induces a longer l_{pz} than a convex TSL of the same G_c.

R-curves can be reproduced by superposing two or more bilinear cohesive laws using a procedure that consists of replicating the layer of cohesive elements while keeping the element connectivity unchanged [2]. The properties of each layer of bilinear cohesive elements are chosen such that the sum of the contributions of all layers has the multi-linear shape of the TSL of interest. For example, the result of superposing two bilinear laws with the same critical displacement jump is a trilinear law, as illustrated in Fig. 1, where the cohesive law of the base layer is defined by its strength (σ_{c0}) and maximum displacement jump (Δ_{f0}). The area underneath the base law corresponds to G_{c0}. The superposed elements represent a "bridging" law defined by maximum elastic bridging strength (σ_{cBr}), maximum effective bridging displacement (Δ_{fBr}) and bridging SERR (G_{cBr}). The penalty stiffness (K) of the bridging law is chosen such that the critical displacement (Δ_c) for the base and the bridging laws are equal, which ensures that the sum of the two laws is trilinear rather than quadrilinear. The sum of the two bilinear laws results in a trilinear traction-separation law that initiates damage at maximum elastic strength (σ_c) and fails when the cohesive strength reduces to zero at Δ_{fBr}. The main advantage of superposing bilinear elements as opposed to constructing a single multilinear TSL is that thermodynamically consistent multilinear cohesive laws capable of mode mixity are difficult to formulate, while most bilinear laws have this capability. The method of superposition has been demonstrated in several problems, including skin/stiffener separation [5] and through-thickness fracture [2].

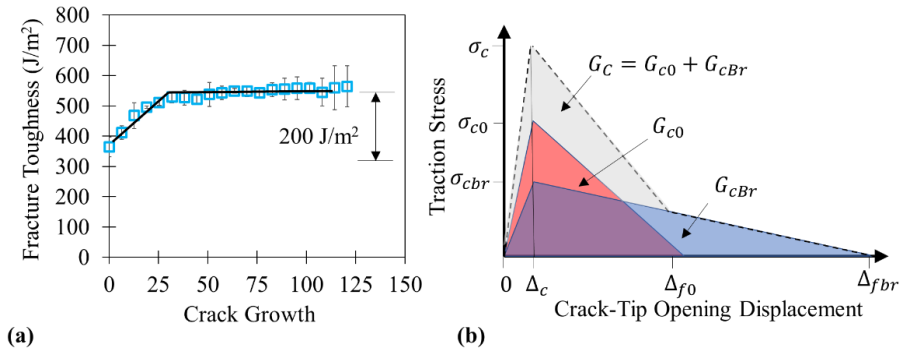

Fig. 1. a) R-curve and b) TSL obtained by superposition of bilinear cohesive laws.

The main disadvantage of CZM approach is that it requires meshes that are much finer than those needed to capture structural deformation. To calculate the SERR

accurately, the cohesive zone length must be discretized with at least three elements. The cohesive zone length (l_{pz}) corresponding to a bilinear cohesive law is approximately [6]

$$l_{pz} \approx \frac{E_{22} G_c}{\sigma_c^2} \tag{1}$$

The fracture process zone length is a function of transverse modulus (E_{22}), the critical SERR (G_c), and the maximum elastic strength (σ_c). The fracture process zone length is inversely proportional to the maximum elastic strength squared. The fracture process zone lengths in aerospace composites are often less than 1 mm. Under large-scale bridging conditions, the maximum elastic bridging strengths (σ_{cBr}) are significantly lower and will result in much larger fracture process zones, thereby allowing much larger elements to be used to simulate bridging conditions.

3 Representing an R-curve response with VCCT

The VCCT approach is an LEFM approach that can be used to predict the propagation of delamination along initially tied surfaces of a delaminated body. In Fig. 2a, a finite element with an initially delaminated interface is shown. The tied surfaces are represented by coincidental nodal pairs (1, 6) and (2, 5). These nodes along the delamination path are released sequentially when the SERR exceeds a critical value: $G_I \geq G_{IC}$. For fracture in mode I, the SERR can be calculated as [3]

$$G_I = \frac{1}{2} \frac{F_{v,2,5}}{b \cdot \Delta a} \Delta w_{1,6}, \tag{2}$$

where the term $F_{v,2,5}$ represents the nodal forces at the crack tip and the term $\Delta w_{1,6}$ is the relative nodal displacements behind the crack tip. In Fig. 2a, the nodal displacement is measured between Nodes 1 and 6. The crack increment, Δa, is the length of element at the crack front and the term b is the width of the DCB specimen. To minimize the oscillations caused by the release of a pair of tied nodes (Nodes 2-5), the closing forces are progressively ramped down at a rate that ensures that the energy dissipated corresponds to G_{IC}, as illustrated in Figure 2b. Since VCCT is an LEFM approach, it cannot represent the large process zones that induce R-curves. However, R-curves can be simulated by specifying $G_{IC}(x, y)$ as a function of nodal position along the delaminating plane. The drawbacks of this approach compared to modeling R-curves as a bridging mechanism include: 1) a dependence on pre-defined propagation paths, 2) the inability to account for changes in the R-curve with specimen thickness, and 3) potential errors in the predicted crack-tip opening displacements in the immediate wake of the delamination front.

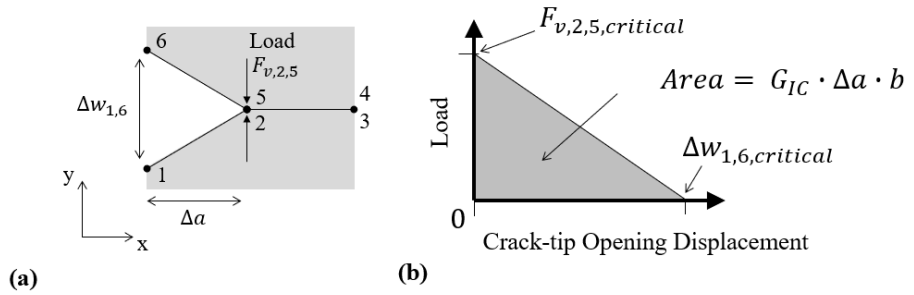

Fig. 2. a) Cracked body at a contact interface and b) force-displacement [7].

4 Representing an R-curve response by combining CZM and VCCT

The CZM approach to represent R-curve responses by the superposition of bilinear cohesive laws is versatile, but the mesh requirements of the approach make CZM intractable for larger structures. These mesh size requirements are set by the lengths of the fracture process zones (l_{pz}s). However, the l_{pz}s associated with each superposed layer of cohesive elements can be extremely different from each other due to the differences in maximum elastic strength, which is identified in Equation 1. The mesh requirements for the superposed CZM approach are determined by the cohesive law with the shortest l_{pz}. This understanding motivated the possibility of replacing the cohesive law with the shortest l_{pz} with VCCT. For this study, the combined approach is illustrated in Figure 3. This approach utilizes a VCCT interface that is in conjunction with cohesive elements. The VCCT interface only considers an initiation criterion based on the critical strain energy release rate measured at initiation. To simulate the R-curve effect, the VCCT interface is superposed with cohesive bridging elements. The properties of the bridging elements are obtained by separating the TSLs into high-strength (HS) and low-strength (LS) components. By enabling the low strength TSLs only in the combined approach, a significantly larger cohesive element can be used to represent R-curve effects during delamination of polymer composites.

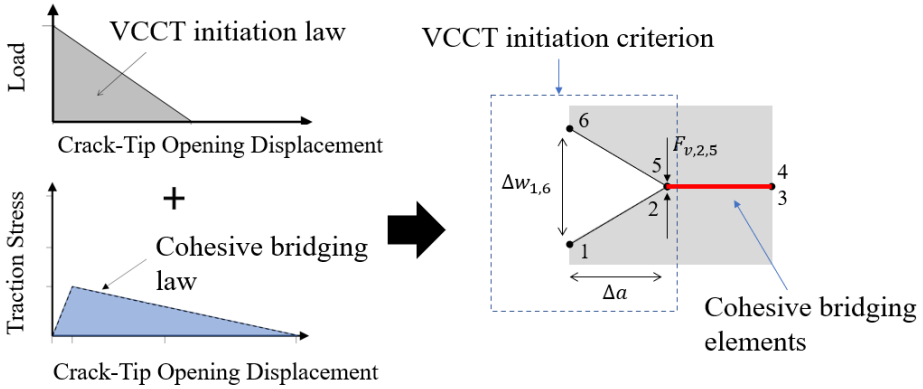

Fig. 3. Combining the initiation law and cohesive bridging laws.

5 Materials, fabrication, and experimental procedure

DCB Specimens were fabricated in accordance with ASTM D5528 [8]. The matrix material used in this study is an out-of-autoclave aromatic epoxy resin system (Hexflow®1078 *, Tg = 178ºC). The epoxy resin system is toughened with 200-nm diameter core-shell rubber particulates, incorporated by the manufacturer. The reinforcement used in this study is made from a dry carbon [0/90] non-crimped (NCF) manufactured by SAERTEX, Inc. Two laminate configurations were considered, $[0/90/90/0]_{3s}$ and $[0/90/90/0]_{9s}$. The resulting cured laminate thicknesses are approximately 5 mm and 15 mm, respectively. The individual plies of the NCF fabric are bound together using a 74-dtex polyester thread in a tricot stitching pattern. A Teflon™ film of 0.0127-mm thickness was used as the crack initiator at the midplane of the laminate and at an initial crack length of approximately 50.8 mm.

The composite laminates were manufactured using a vacuum-assisted resin transfer molding (VARTM) process [9, 10]. Resin infusion was performed at 88ºC to minimize the viscosity of the resin. The resin was held under vacuum at 88ºC for one hour prior to infusion and underwent a thin-film degassing process. During this degassing process, the resin was stirred at 300 RPM in the resin tank for approximately 20 minutes to remove air bubbles. After infusion, the temperature was held at 149ºC for six hours, increased to 177ºC for two hours, and allowed to cool to ambient temperature. The composite laminates were sectioned after cure to fabricate DCB test specimens as illustrated in Fig. 4. Mounting blocks were bonded above the crack-initiating plane using 9394 Hysol Loctite™ adhesive.

The DCB tests were conducted based on ASTM D5528 using an Instron 8872 hydraulic test frame. The specimens were loaded at a displacement rate of 0.5 mm/min with a 1 kN load cell. The crack lengths were measured visually with the aid of a camera

* The use of trademarks or names of manufacturers in this report is for accurate reporting and does not constitute an official endorsement, either expressed or implied, of such products or manufacturers by the National Aeronautics and Space Administration.

system. The edge of each specimen was marked in 6.35-mm intervals to monitor crack growth. The DCB specimens were loaded until the displacement reached 50.8 mm or the specimen delaminated completely along its length. A total of three tests per laminate thickness was performed. After tests, the initial crack lengths were measured by measuring the length of the Teflon placed in the preform to the specimen edge. The initial crack lengths were measured to be 27.3 mm and 32.3 mm for the 5-mm and 15-mm thick specimens, respectively.

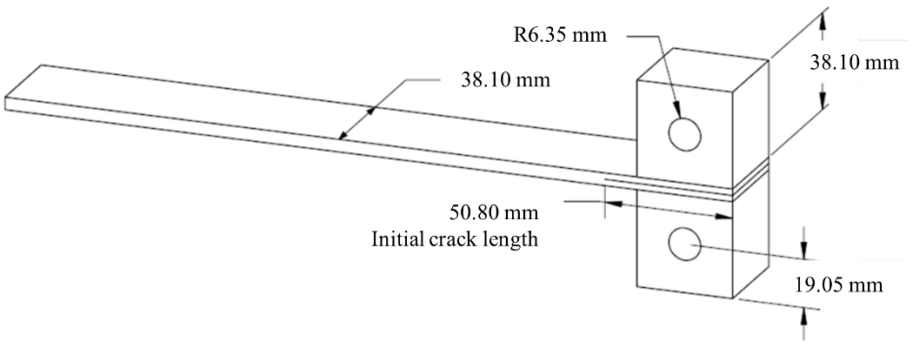

Fig. 4. Double cantilevered beam (DCB) specimen schematic.

6 Estimation of mode I fracture energy

The experimental mode I SERR G_I was estimated according to the ASTM D5528 Standard using the modified compliance calibration method (MCC) [8] as

$$G_I = \frac{3P^2C^{2/3}}{2A_1bh}, \tag{3}$$

where P and C are the reactive load and compliance, respectively. The compliance is determined by the ratio of the applied displacement over the load. The specimen width and thickness are denoted as b and h, respectively. The parameter A_1 is a calibration parameter that is the slope of the normalized crack length a/h as a linear function of the cube root of the compliance ($C^{1/3}$). This parameter is determined experimentally for each DCB test specimen. The normalized crack length with respect to the cube-root of the compliance is shown for both specimen thicknesses (5 mm and 15 mm) in Fig. 5. As expected, a linear trend is observed for both specimen thicknesses.

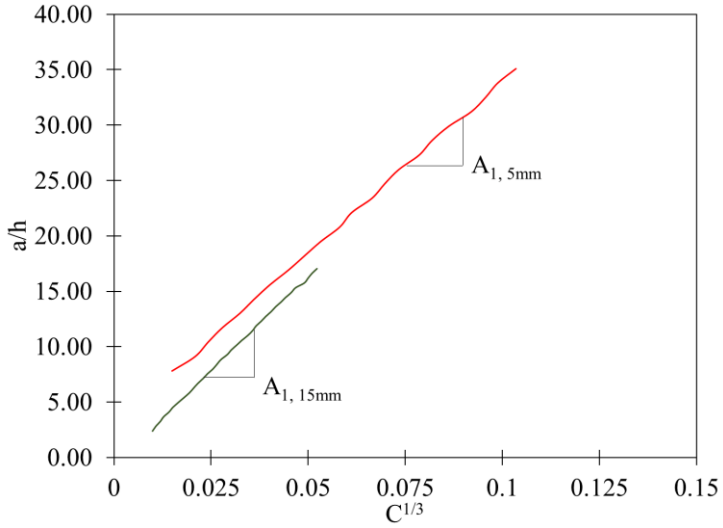

Fig. 5. Normalized crack length as a function of the cube root of the compliance.

In fracture problems with large process zones, J-integral solutions provide more accurate values of the SERR than methods based on LEFM such as MCC. The J-integral approach does not require measuring the crack length, but it does require recording the rotations, θ, of the specimen arms at the load-application point, i.e.,

$$J_I = \frac{2P\theta}{b}. \tag{4}$$

The rotations were not recorded during the experimental test program, but they can easily be obtained from the analysis results. To evaluate the accuracy of the SERR calculated by the MCC method, the SERR as a function of crack length is calculated using both methods. For one of the 15-mm simulations, a comparison between the MCC method and J-integral response is shown in Fig. 6. At initiation, both solutions yielded identical results. As delamination increases and a larger fracture process zones develops, the MCC solution underpredicts the J-integral method. At the maximum observed crack length, a 6.8% difference was observed between the two solutions, which is considered acceptable for the analysis herein.

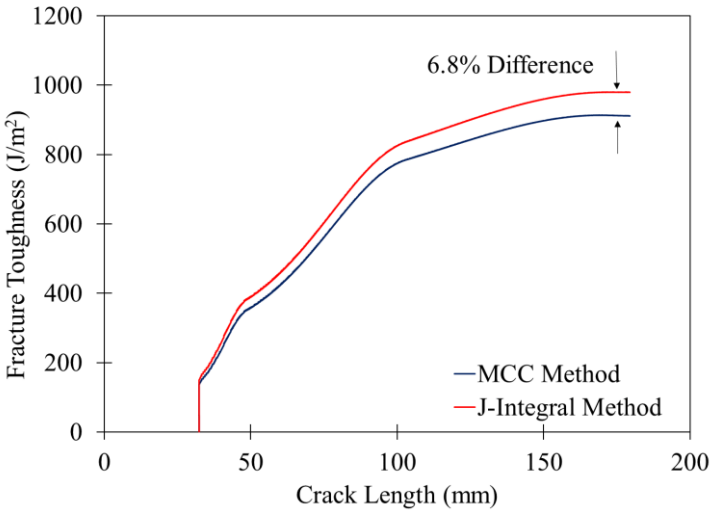

Fig. 6. Fracture toughness as a function of crack length for the MCC and J-Integral methods.

7 Computational approach

Implicit two-dimensional finite element analyses were conducted using Abaqus/Standard v2022 commercial software. Three analysis types were conducted to simulate delamination at the midplane of each laminate: a VCCT analysis, a CZM analysis, and an analysis that combines VCCT and CZM. The VCCT analysis was implemented using a contact interface at the midplane of the laminate, whereas the CZM used zero-thickness cohesive elements at the midplane of the laminate. The composite mesh was simulated using hexahedral elements (C3D8I) with incompatible modes. The combined VCCT/CZM approach utilized contact at the interface and cohesive elements to simulate delamination. All analyses were performed using the same DCB finite element model for both laminate thicknesses (5 mm and 15 mm). The elastic properties of the cured composite are shown in Table 1. The fracture parameters for the VCCT and CZM approaches are shown in Tables 2 and 3 for the 5-mm and 15-mm simulations, respectively. The critical SERR, maximum elastic strength, and penalty stiffness are denoted as G_{Ic}, σ_t, and K, respectively. The process for determination of these fracture parameters is provided in the following section for determination of bridging laws. For the VCCT approach, the SERR as a function of crack length was directly incorporated into the finite element model to simulate R-curve effects. The CZM approach and the combined VCCT/CZM approach used superposed bilinear TSLs to estimate the R-curve effect.

The finite element model with the displacement boundary conditions is shown in Fig. 7. Above and below the disbond region, a 7.5-mm applied displacement is used to simulate the loading acting on the DCB specimen. Additional x-direction constraints are added to prevent rigid body displacement and rotation. The initial disbond lengths of the 5-mm and 15-mm specimens are 25.0 mm and 32.3 mm, respectively. To help

with model convergence, a viscoelastic regularization coefficient of 1.0E-6 was used for the CZM and combined VCCT/cohesive model. The contact tractions were set to gradually release during succeeding time increments after the critical SERR was reached using the VCCT method. To evaluate the computational efficiency of the modeling approaches, the element lengths along the delaminating plane were increased from 0.1 mm to 10 mm. The length of the cohesive elements and structural elements representing the composite were maintained equal during the analysis.

Table 1. Elastic properties of finite element model [11].

Property	**Unit**	**Value**
$E_{11}=E_{22}$	GPa	56.6
E_{33}	GPa	8.64
$G_{12}=G_{13}$	GPa	4.66
G_{23}	GPa	4.95
v_{12}	mm/mm	0.06
$v_{13}=v_{23}$	mm/mm	0.25

Table 2. Fracture parameters for the 5 mm simulations.

Model	G_{Ic} **(N/mm)**	σ_t **(MPa)**	K **(MPa/mm)**
VCCT (HS)	0.150	-	-
Cohesive			
TSL-1 (HS)	0.150	89.0	2.00E+05
TSL-2 (LS)	0.250	2.00	4.47E+02
TSL-3 (LS)	0.150	0.20	8.00E-01

Table 3. Fracture parameters for the 15 mm simulations.

Model	G_{Ic} **(N/mm)**	σ_t **(MPa)**	K **(MPa/mm)**
VCCT (HS)	0.150	-	-
Cohesive			
TSL-1 (HS)	0.150	89.0	2.00E+05
TSL-2 (LS)	0.300	25.0	5.59E+03
TSL-3 (LS)	0.350	0.30	1.25E+01
TSL-4 (LS)	0.200	0.03	1.29E-02

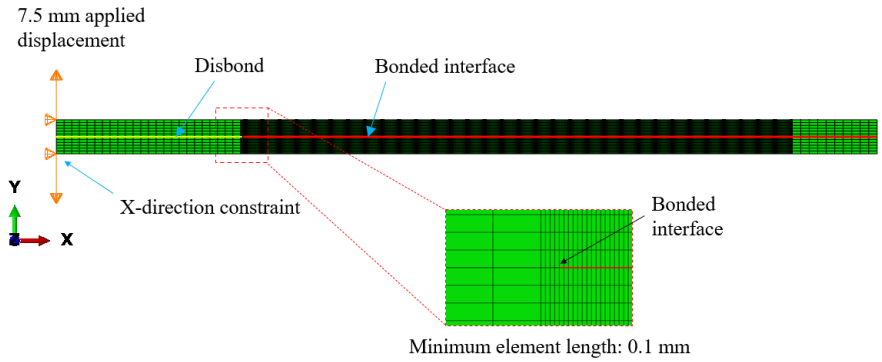

Fig. 7. Finite element model with boundary conditions.

8 Determination of bridging laws

The determination of the traction-separation laws (TSL) to represent R-curves can be challenging. Monsef et al. [12] proposed a technique to extract the TSL corresponding to an R-curve by fitting the load-displacement curve. In a similar manner, an iterative method based on the predicted load-displacement curve and the predicted R-curves was used in the present effort to estimate the bridging TSLs. A flow chart of the process to determine the bridging laws is provided in Fig. 8. Estimates of the J-integral as a function of the crack-tip opening displacements were initially made using the VCCT method. The corresponding traction stresses were determined by calculating the derivative of the J-integral with respect to the crack-tip opening displacement. To assist in reducing the variation in the predicted TSL, a moving average technique was used to filter the noise in the initial predicted TSL. Once the initial TSL was determined, bilinear TSLs were superposed to approximate the VCCT solution. Once the initial bilinear TSLs were determined, a CZM was developed. The predicted load-displacement response from the CZM approach was compared to the experimental data. The maximum elastic strengths and fracture toughnesses were adjusted to match the load-displacement curves and R-curves. The final fracture parameters for all TSLs and specimen thickness are provided in Tables 2 and 3.

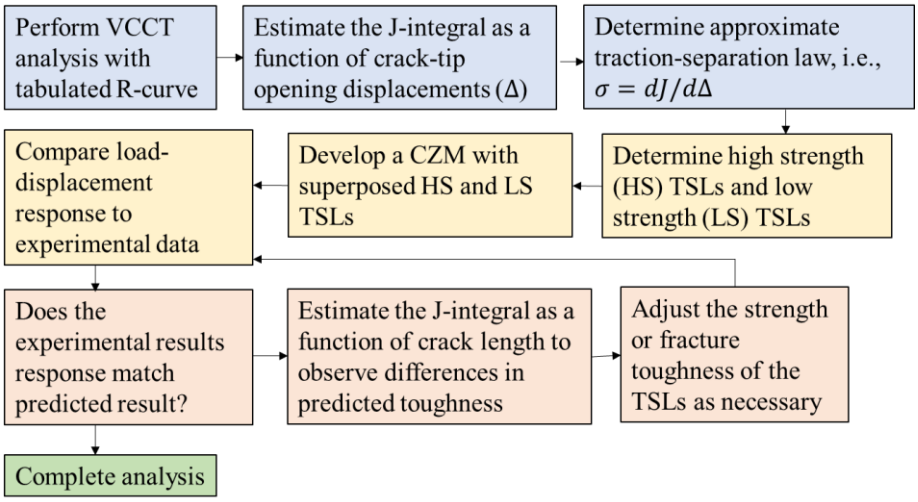

Fig. 8. Flow chart to determine HS and LS TSLs.

9 Results and discussion

The experimental and predicted force-displacement curves for both specimen configurations are shown in Fig. 9. Initially, all samples exhibit a linear increase in the load until the initiation of delamination occurs. A reduction in the slope of the load-displacement response is observed after delamination initiation until a maximum load is achieved. All specimens exhibited stable load-shedding during delamination propagation after the maximum load was reached. This pattern is primarily due to the increased distance from the crack front to the location of the applied displacement, requiring less load to develop the necessary tensile stresses to progress the crack front. Increasing the laminate thickness increases the reactive load when delamination occurs due to an increase in flexural rigidity. The predicted load for both laminate thicknesses and all analysis approaches generally show good agreement (within 10%) to the corresponding experimental value. For the 5-mm specimen, each solution shows excellent agreement (within 2%) with respect to the load-displacement response. For the 15-mm specimen, VCCT overpredicted the peak load by approximately 8.3%. The CZM and combined VCCT/CZM produced identical results for all cases and produced a better correlation to the experimental value (within 2%). The VCCT solution showed greater agreement during steady-state delamination during load-shedding after the maximum peak load is achieved.

In Fig. 10, the crack length as a function of the applied displacement is shown. Increasing the applied displacement showed a proportional increase in the crack length and a gradual decrease in the slope of the crack length response is observed. Increasing the specimen thickness from 5 mm to 15 mm resulted in a significant increase in crack growth. At the maximum applied displacement of 15 mm, crack growth in the 15-mm thick specimen is approximately two times greater than the 5-mm specimen. The

predicted crack length for both laminate thicknesses and all analysis approaches generally show good agreement (within 10%) to the corresponding experimental value.

The experimental and predicted SERR as a function of the crack length for both laminate thicknesses are shown in Fig. 11. The 5-mm DCB specimens exhibit an initial increase in the SERR and convergences asymptotically to a SERR that is 50% greater than the initiation value as the crack length increases. The 15-mm DCB specimen exhibits approximately five times greater SERR than its initiation value. This increase in the SERR is primarily attributed to carbon fiber bridging and additional toughening mechanisms associated with the core-shell rubber particulates used within the Hexcel 1078 resin system [13]. In addition, an examination of the delamination surfaces revealed unique bundles of polyester thread that bridge the delamination plane. This polyester thread is a warp-knit stitch that is needed to bind the dry carbon fiber plies of different orientations together for handling during fabrication prior to resin infusion. This bridging of the delamination plane significantly increases the SERR and fracture process zone length. Additionally, the predicted SERR calculated using the J-integral approach for the VCCT, CZM, and combined VCCT/CZM solutions also showed good agreement to the experimental SERR estimates. The results are indicative that a VCCT solution combined with bridging cohesive elements can accurately predict crack growth that undergoes large-scale bridging. Furthermore, the representation of crack initiation using a VCCT approach results in using cohesive elements that have much lower maximum elastic strengths (<25 MPa) prior to their failure as compared to the CZM-only solution (89 MPa). This indicates that larger cohesive elements, on the order of those used in structural scale models (> 10.0 mm), can be used to simulate large-scale bridging conditions efficiently.

The computational cost for select element lengths (L_e = 0.1 mm to 10 mm) and analysis types (VCCT, Cohesive, and VCCT with Cohesive) are shown in Table 4. For all solutions, decreasing the DOF of the finite element model decreased the overall computational time. A CZM-only finite element model took approximately twice as long as a VCCT-only finite element model for a 0.1-mm element length. It's important to note that improvements in the computational time can be made by increasing the viscoelastic regularization coefficient. However, only a value of 1.0E-6 is considered herein. Additionally, the CZM-only approach was not able to reach convergence for element lengths greater than 1 mm. The combined VCCT/CZM finite element model had the same relative computational cost (1 hour and 39 minutes) as the VCCT solution using an element length of 0.1 mm. Increasing the element size from 0.1 mm to 10 mm resulted in a nearly equivalent computational time for both the VCCT and combined VCCT/CZM approaches. The VCCT and combined VCCT/CZM approaches took approximately seven to eight minutes using an element length of 10 mm.

In Fig. 12, the predicted load-displacement response for all element lengths and analysis types is shown. For the CZM-only approach, increasing the element length from 0.1 mm to 1 mm resulted in overpredicting the peak load at delamination initiation by approximately 200%. For fine meshes (0.1 mm and 1 mm), a smooth load-displacement behavior was observed for all modeling approaches. Increasing the element length above 2.5 mm resulted in unstable crack growth, and a saw-tooth behavior was observed in the load-displacement response for VCCT and VCCT/CZM approaches.

Unlike the CZM-only approach, the peak loads of VCCT and VCCT/CZM predictions were approximately within 5% to 16% of the baseline solutions that used an element length of 0.1 mm. These results are indicative that significantly large cohesive elements can be used to efficiently simulate large-scale bridging conditions when used in combination with the VCCT approach. Furthermore, some filtering may be required when using relatively large elements (5 mm or greater) due to the saw-sooth behavior observed in the load-displacement response.

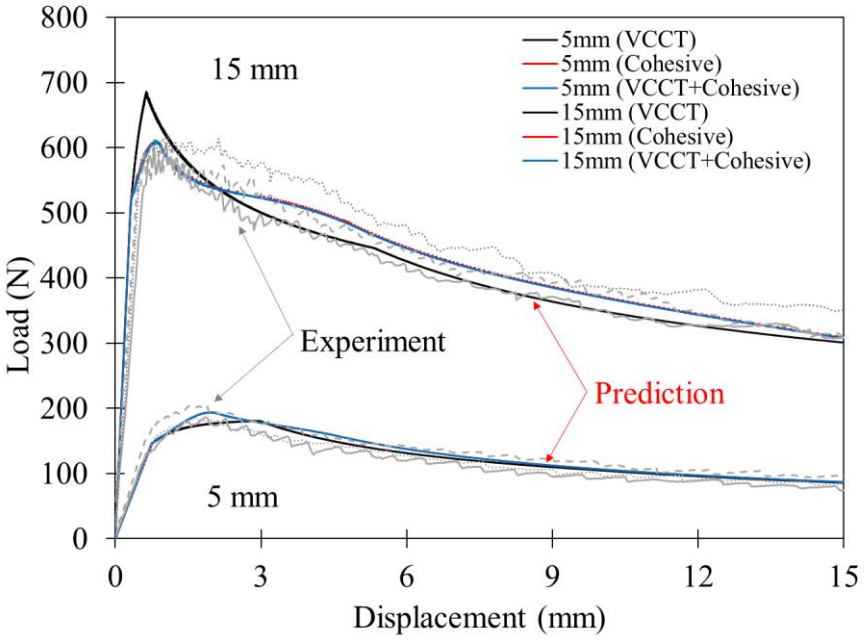

Fig. 9. Experimental and predicted load as a function of the applied displacement for each laminate thickness and analysis approach.

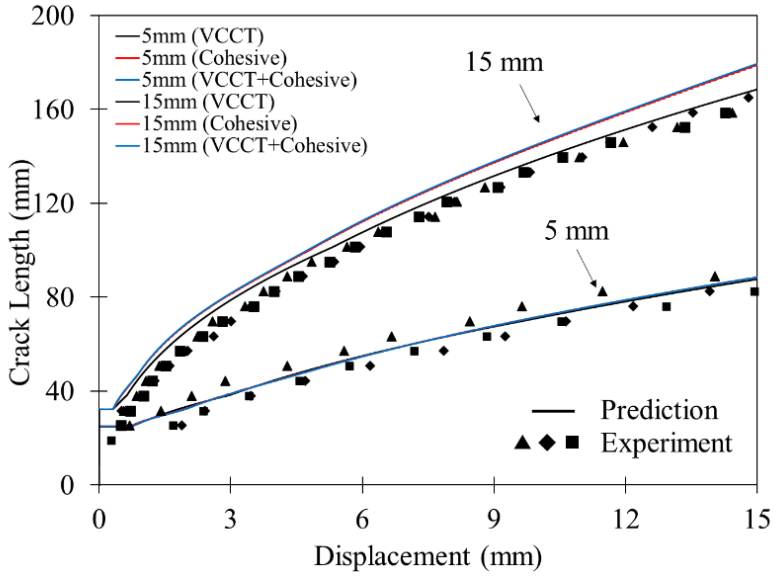

Fig. 10. Experimental and predicted crack length as a function of the applied displacement for each laminate thickness and analysis approach.

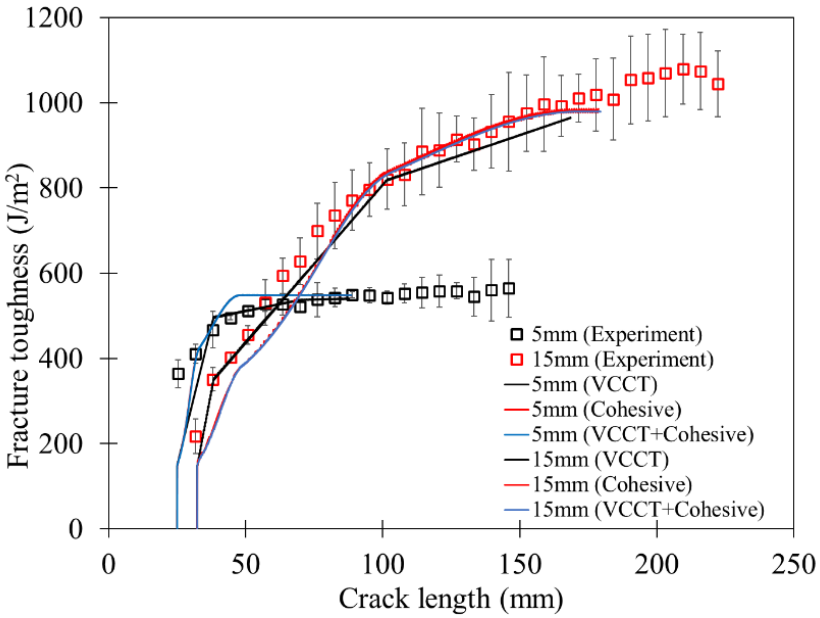

Fig. 11. Experimental and predicted SERR as a function of the applied displacement for each laminate thickness and analysis approach.

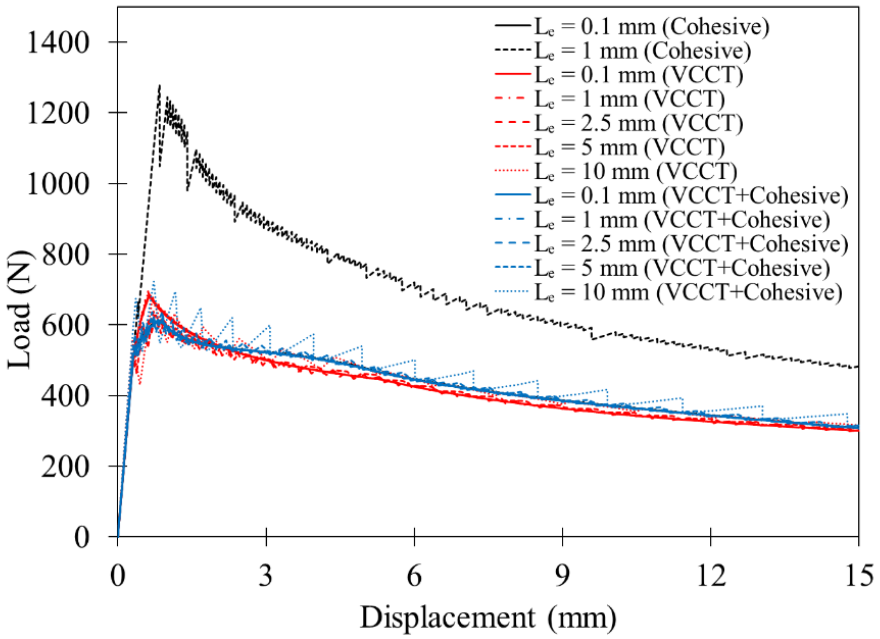

Fig. 12. Predicted load as a function the applied displacement for select element lengths (L_e = 0.1 mm to 10 mm) and analysis types (VCCT, Cohesive, and VCCT/Cohesive).

Table 4. Computational cost for select element lengths and analysis types.

Element Length (L_e)	Time Completed (Hr:Min)			No. of Degrees of Freedom
	VCCT	Cohesive	Combined	
0.1 mm	1:39	3:04	1:39	54950
1.0 mm	0:24	1:05	0:44	16660
2.5 mm	0:09	n/a	0:20	6790
5 mm	0:10	n/a	0:11	3710
10 mm	0:07	n/a	0:08	1890

10 Conclusions

In this study, a methodology is proposed that combines the VCCT approach with cohesive elements to predict delamination in problems with R-curve responses. The approach consists of separating the cohesive TSL into high and low-strength responses. The high strength portion, which is responsible for the high mesh refinement required for the entire analysis, is substituted by VCCT, which has lower mesh requirements. The remaining lower-strength portion of the TSL is ideally suited to represent bridging

and other toughening mechanisms that induce an R-curve response. The efficacy of the VCCT/CZM solution is compared to a VCCT-only solution and a CZM-only solution in addition to experimental data. The following observations are made:

- The 5-mm and 15-mm specimens showed varying degrees of large-scale bridging, which is observed by the increases in the SERR as a function of crack length. The 5-mm and 15-mm specimens yielded SERRs during propagation that were two times and five times larger, respectively, than the SERRs observed at initiation.
- The predicted load and crack growth for all solutions generally showed good agreement (within 10%) with each other and with experimental data. The VCCT solution over-predicted the load-displacement response by 8.3%, which is attributed to the linear-elastic assumptions using the VCCT-only approach.
- The VCCT/CZM combined approach matches exactly the CZM solution for element sizes of 0.1 mm.
- The computational time of the combined VCCT/CZM approach is nearly equivalent to a VCCT-only approach. For large element lengths, a saw-tooth pattern in the load-displacement results is observed for both solutions.

The results herein suggest that the VCCT approach can be used to efficiently predict large-scale bridging conditions when combined with the cohesive element approach.

References

1. Drake, D.A., Sullivan, R.W., Lovejoy, A.E., Clay, S.B., Jegley, D.C.: Influence of stitching on the out-of-plane behavior of composite materials – A mechanistic review. Journal of Composite Materials. 55, 3307–3321 (2021).
2. Dávila, C.G., Rose, C.A., Camanho, P.P.: A procedure for superposing linear cohesive laws to represent multiple damage mechanisms in the fracture of composites. Int. J. Fracture. 158, 211–223 (2009).
3. Krueger, R.: Viritual crack closure technique: history, approach, and applications. Appl Mech Rev. 57, 109–143 (2004). https://doi.org/10.1115/1.1595677
4. Drake, D.A., V. De Carvalho, N., Lovejoy, A.E.: Reduction in Computational Cost of Progressive Failure Analysis of Composite Structures. Presented at the American Society for Composites (ASC) 38th Annual Technical Conference , Boston, MA September 17 (2023)
5. Dávila, C.G., Ratcliffe, J.G.: Quasi-static and Fatigue Delamination at Tape/Fabric Interfaces. AIAA SciTech 2020 Conference. , Orlando, FL (2020)
6. Turon, A., Dávila, C.G., Camanho, P.P., Costa, J.: An engineering solution for mesh size effects in the simulation of delamination using cohesive zone models. Engineering Fracture Mechanics. 74, 1665–1682 (2007).
7. Abaqus/Standard User's Manual, Version 2022
8. ASTM D5528-01: Standard Test Method for Mode I Interlaminar Fracture Toughness of Unidirectional Fiber-Reinforced Polymer Matrix Composites. In: Annual Book of ASTM Standards. American Society for Testing and Materials, West Conshohocken, PA (2002)

9. Agarwal, B., Broutman, L., Chandrashekhara, K.: Analysis and Performance of Fiber Composites. John Wiley & Sons, Inc. (2006)
10. API 1078 - Aircraft Structural VARTM Resin Technical Datasheet. Applied Poleramic, Inc.
11. Drake, D.A., Sullivan, R.W., Clay, S.: On the use of a trilinear traction-separation law to represent stitch failure in stitched sandwich composites. Jnl of Sandwich Structures & Materials. 24, 1367–1384 (2022).
12. Abdel Monsef, S., Ortega, A., Turon, A., Maimí, P., Renart, J.: An efficient method to extract a mode I cohesive law for bonded joints using the double cantilever beam test. Composites Part B: Engineering. 178, 107424 (2019).
13. Quan, D., Ivankovic, A.: Effect of core–shell rubber (CSR) nano-particles on mechanical properties and fracture toughness of an epoxy polymer. Polymer. 66, 16–28 (2015).